Combating Impairments in Multi-carrier Systems: A Compressed Sensing Approach

Thesis by

Shamael A. Al-Shuhail

In Partial Fulfillment of the Requirements

For the Degree of

Masters of Science

King Abdullah University of Science and Technology, Thuwal,

Kingdom of Saudi Arabia

May, 2015

The thesis of Shamael Al-Shuhail is approved by the examination committee

Committee Chairperson: Dr. Tareq Alnaffouri

Committee Member: Dr. Mohamed-Slim Alouini

Committee Member: Dr. Basem Shihada

Committee Member: Dr. Hamid Bahrami

ABSTRACT

Combating Impairments in Multi-carrier Systems: A Compressed Sensing Approach

Shamael A. Al-Shuhail

Multi-carrier systems suffer from several impairments, and communication system engineers use powerful signal processing tools to combat these impairments and keep up with the capacity/rate demands. Compressed sensing (CS) is one such tool that allows recovering any sparse signal, requiring only a few measurements in a domain that is incoherent with the domain of sparsity. Almost all signals of interest have some degree of sparsity, and in this work we utilize the sparsity of impairments in orthogonal frequency division multiplexing (OFDM) and its variants (i.e., orthogonal frequency division multiplexing access (OFDMA) and single-carrier frequency-division multiple access (SC-FDMA)) to combat them using CS. We start with the problem of peak-to-average power ratio (PAPR) reduction in OFDM. OFDM signals suffer from high PAPR and clipping is the simplest PAPR reduction scheme. However, clipping introduces inband distortions that result in compromised

performance and hence needs to be mitigated at the receiver. Due to the high PAPR nature of the OFDM signal, only a few instances are clipped, these clipping distortions can be recovered at the receiver by employing C-S. We then extend the proposed clipping recovery scheme to an interleaved OFDMA system. Interleaved OFDMA presents a special structure that result in only self-inflicted clipping distortions. In this work, we prove that distortions do not spread over multiple users (while utilizing interleaved carrier assignment in OFDMA) and construct a CS system that recovers the clipping distortions on each user. Finally, we address the problem of narrowband interference (NBI) in SC-FDMA. Unlike OFDM and OFDMA systems, SC-FDMA does not suffer from high PAPR, but (as the data is encoded in time domain) is seriously vulnerable to information loss owing to NBI. Utilizing the sparse nature of NBI (in frequency domain) we combat its effect on SC-FDMA system by CS recovery.

TABLE OF CONTENTS

LIST OF ABBREVIATIONS

OFDM Orthogonal Frequency Division Multiplexing

OFDMA Orthogonal Frequency Division Multiplexing Access

PAPR Peak-to-Average Power Ratio

SC-FDMA Single-Carrier Frequency-Division Multiple Access

NBI Narrowband Interference

CS Compressive Sensing

IT Iterative Thresholding

OMP Orthogonal Matching Pursuit

FBMP Fast Bayesian Matching Pursuit

SIMO Single-Input Multi-Output

SABMP Support Agnostic Bayesian Matching Pursuit

ItML Iterative Maximum-Likelihood

CR Clipping Ratio

DFT Discrete Fourier Transform

IDFT Inverse Discrete Fourier Transform

AWGN Additive White Gaussian Noise

IHT Iterative Hard Thresholding

IST Iterative Soft Thresholding

ML Maximum Likelihood

BS Base Station

QAM Quadrature Amplitude Modulation

BER Bit-Error-Rate

E_b/N_0 Energy per Bit to Noise Power Spectral Density Ratio

dB Decibel

ZF-FDE Zero Forcing-Frequency Domain Equalization

MMSE-FDE Minimum Mean Square Error-Frequency Domain Equalization

MMV Multiple Measurement Vector

SIR Signal-to-Interference

SMV Single Measurement Vector

MRC Maximal Ratio Combining

LIST OF FIGURES

Chapter 1

Introduction

OFDM is a widely used modulation technique adopted by many wired and wireless technologies. It is a multi-carrier modulation technique based on modulating a number of orthogonal carriers [1]. OFDM can be extended to allow access to multiple users hence resulting in OFDMA. OFDMA assigns a subset of available subcarriers for each user. Because of the orthogonal nature of the subcarriers, interference is eliminated between users [1]. OFDM and OFDMA systems offer a considerably high spectral efficiency, multipath delay spread tolerance, immunity to the frequency selective fading channels and power efficiency [2], [3]. On the other hand, high PAPR is the main disadvantage of OFDM signals. High PAPR in mobile communications uplink causes distortion to the power amplifier at the transmitters side [1].

SC-FDMA is a modification of OFDM that achieves the same throughput performance and complexity as in OFDM [4], [5], [6]. The advantage of SC-FDMA over OFDM is its low PAPR. SC-FDMA also has an additional advantage for removing the influence of multipath effect [7]. However,

the wideband nature of SC-FDMA makes it highly vulnerable to NBI. N-BI sources are other devices operating in the same spectrum (e.g., cordless phones, garage openers etc.) or other systems operating in a cognitive manner [8].

To solve the PAPR problem in OFDM and OFDMA systems, one can apply simple clipping at the transmitter and recover the clipping signal using a recovery technique at the receiver's side. The clipping signal is observed to be sparse by nature i.e., non-zero elements only at a relatively small number of locations in the signal. As for solving the NBI problem in SC-FDMA, the NBI effect needs to be estimated then mitigated to recover the original signal back at the receiver's side. The NBI signal is observed to be sparse as well (albeit in frequency domain), due to the small number of active sources actually interfering with the SC-FDMA signal. Hence, both problems can be looked at as sparse signal recovery problems. CS techniques have been proposed as a tool for recovering sparse signals. Hence, solving both the problems of PAPR reduction [9], [10] and NBI cancellation [11], [12] can be looked at as sparse signal recovery problems.

There have been many CS schemes proposed e.g., ℓ_1-minimization [9] and Bayesian schemes [13]. However, CS recovery schemes have two main issues, the computational complexity of the schemes and not utilizing prior information. To solve the complexity issue, many authors have proposed greedy algorithms that are seen to operate simpler and faster than any other CS schemes. Greedy algorithms such as, IT [14] and OMP [15]. As for the prior information issue, many other CS recovery schemes proposed, utilize available information to further enhance and simplify the recovery process.

Algorithms such as, Bayesian schemes use the fact that the noise is Gaussian [16] and the FBMP algorithm utilizes the fact that the sparse unknown is Gaussian as well as noise [17].

This thesis is organized into 3 chapters and below we highlight the contributions of each:

Chapter 2: Iterative Thresholding Recovery for PAPR Reduction in OFDM Signals: We use thresholding on OFDM signals for PAPR reduction. We then seek to reconstruct the clipping signal at the receiver's side by using the IT algorithm. We modify the IT algorithm by taking into account phase information to enhance the recovery. The prior data that the algorithm uses is replaced with reliable data by following a data-aided approach. Our work is further extended to a SIMO system.

Chapter 3: Clipping Distortion Mitigation in Clipped OFDMA Systems: In this chapter, we use the clipping algorithm on the OFDMA system. With many users subjected to clipping, clipping distortions tend to overlap in frequency domain. However, it was found that for the special case of interleaved OFDMA the problem of overlapping clipping distortion is shunned. We also present a mathematical proof authenticating the observation that clipping distortions are self inflicted for interleaved OFDMA. Later we deploy CS as a tool for clipping recovery in OFDMA.

Chapter 4: Narrowband Interference Cancellation in SC-FDMA Systems: We use a CS scheme known as SABMP to estimate and mitigate the effect of NBI on the SC-FDMA signal. We further employ a data-aided approach to increase the system spectral efficiency. Additionally, we extend our work to a SIMO system i.e., the more practical case.

Chapter 2

Iterative Thresholding Recovery for PAPR Reduction in OFDM Signals

2.1 Introduction

OFDM is a widely used modulation technique to transmit digital data through wireless channels. Though it has many advantages, such as its robustness against intersymbol interference and fading, simplified channel equalization, and spectral efficiency, its primary drawback is high PAPR [18]. The reason behind the high PAPR is that the signal in the time domain is the sum of many narrowband signals, resulting in very high magnitudes at some time instances [19]. The high PAPR signal results in distortions when the transmitted signal is subjected to a transmitter power amplifier.

Many techniques have been proposed to reduce the PAPR. Some exam-

ples are phase optimization [20], nonlinear companding transforms [21], Tone Reservation and Tone injection [22, 23]. One of the simplest approaches used for PAPR reduction is clipping. Clipping is applied on relatively few parts of the signal because the probability of high peaks is low [24].

Due to the sparsity of the clipping signal, CS techniques have been used for PAPR reduction e.g., [9, 10]. According to [25], at most one clipping occurs per OFDM symbol, and hence the receiver must estimate two parameters of the clipping signal: location and size. There has been a number of publications that propose recovery schemes for clipped OFDM signals. One of these approaches was developed in [26], the ItML. Another example is [9] which was ℓ_1-minimization. The ItML algorithm is simple and was seen to have good recovery of the clipped OFDM signal. However, for enhanced recovery one needs to use all information that aides in the estimation of the clipping signal. ItML does not take advantage of such *a priori* information. In [9] the authors make use of the fact that the clipping signal is sparse by nature and use CS recovery, however this approach is known to be computationally complex.

Our aim here is to develop a clipping recovery algorithm that uses maximum information to enhance the recovery process, runs faster than other CS schemes and follows a simple methodology. Hence, we use a CS algorithm that is known as IT [14]. In contrast with convex optimization that are used to find near-optimal estimates of the sparse signal, the IT algorithm is a greedy approach that is faster and finds similar bounds to the convex optimization methods for the estimate of the sparse signals [27]. We then compare it to the ItML algorithm in terms of performance.

The remainder of this chapter is organized as follows. Section 2.2 introduces the data model of an OFDM signal subjected to clipping at the transmitter. In section 2.3 the operation of the IT and ItML algorithms is presented. Section 2.4 modifies the CS model by taking into account additional information to enhance the performance. We further extend the recovery scheme to a SIMO system presented in section 2.5. Finally, we illustrate and analyze our numerical findings in Section 2.6.

2.2 Data Model

In an OFDM system [28], N symbols $\{X_k, k = 0, 1, ..., N-1\}$ are formed into one block with each symbol modulating one subcarrier from a set of subcarriers $\{f_n, n = 0, 1, ..., N-1\}$ with equal frequency separation $1/T$, where T is the original symbol period. Hence, the resulting complex packet of the transmitted OFDM signals can be expressed as the following:

$$x_n = \frac{1}{\sqrt{N}} \sum_{k=0}^{N-1} X_k \exp\left(j\frac{2\pi kn}{N}\right) \qquad 0 \le k \le N-1 \tag{2.1}$$

The transmitted signal's PAPR can be expressed as following:

$$\text{PAPR} = \frac{\max_{0\le n\le N-1} \mid x_n \mid^2}{\text{E}\{\mid x_n \mid^2\}} \tag{2.2}$$

The clipping algorithm basically clips the parts of the signal where it exceeds a certain predetermined limit γ , also know as the clipping threshold [29]. The clipping operation can be mathematically written as [30]:

$$x_p(i) = \begin{cases} \gamma \exp\left(j\angle x(i)\right) & \text{if } \mid x(i) \mid > \gamma \\ x(i) & \text{otherwise} \end{cases} \tag{2.3}$$

where $x_p(i)$ is the i^{th} element of the signal after clipping, and $\angle x(i)$ is the phase of the original signal $x(i)$. According to [30], the clipping threshold γ is related to the CR as CR $= \gamma/\sigma$, where σ is the root mean squared power of the transmitted OFDM signal.

Let us consider the clipping signal that was cut-off from $x(i)$ to be $c(i)$. It is noticed that $\mathbf{c}$ has non-zero elements only at locations where clipping occurred. $\mathbf{c}$ must be anti-phased with $\mathbf{x}$ on the clipping locations. This results in the following expression:

$$x_p(i) = x(i) + c(i) \tag{2.4}$$

When the clipped signal $\mathbf{x}_p$ is received, the receiver needs to estimate the clipping part $\mathbf{c}$ to reconstruct the original signal $\mathbf{x}$ back.

The OFDM system model is designed to transmit the clipped signal $\mathbf{x}_p$ through a channel of length L with impulse response $\mathbf{h} = \{h(0), h(1), ..., h(L-1)\}^T$. Hence, the received time domain signal can be expressed as $\mathbf{y} = \mathbf{H}\mathbf{x}_p$, where $\mathbf{H}$ is the circulant channel matrix which can be diagonalized using the DFT matrix $\mathbf{F}$ and is written as $\mathbf{H} = \mathbf{F}^H\mathbf{D}\mathbf{F}$. Where $\mathbf{D}$ is a diagonal matrix with the partial Fourier transform of the impulse response i.e., $\bar{\mathbf{F}}\mathbf{h}$ on its diagonal. The received frequency domain signal can be written as

$$\mathbf{Y} = \mathbf{D}\mathbf{X}_p + \mathbf{Z} = \mathbf{D}(\mathbf{X} + \mathbf{C}) + \mathbf{Z} \tag{2.5}$$

The channel output $\mathbf{Y}$ consists of the clipped signal plus AWGN, $\mathbf{Z} \sim \mathcal{N}(0, \sigma_z^2\mathbf{I}_{NxN})$. Specifically $\mathbf{C}, \mathbf{X}$, and $\mathbf{X}_p$ are the Fourier Transforms of $\mathbf{c}, \mathbf{x}$, and $\mathbf{x}_p$ respectively. When we further extend (2.5) to an equation with sparse unknown we start with $\mathbf{Y} - \mathbf{D}\mathbf{X} = \mathbf{D}\mathbf{C} + \mathbf{Z}$. By reserving some carriers, meaning that $\mathbf{X} = 0$ on some carriers, we are able to get the measurement vector

for the CS model. The number of reserved tones is said to be m. The same goes to $\mathbf{D}$, the matrix will only have the rows corresponding to those reserved tones, changing the size of $\mathbf{D}_m$ to be $m \times N$. Hence, we get $\mathbf{Y}_m = \mathbf{D}_m\mathbf{C} + \mathbf{Z}$. Since our sparse unknown is $\mathbf{c}$, we can express $\mathbf{C}$ in terms of $\mathbf{c}$ as $\mathbf{C} = \mathbf{F}\mathbf{c}$. This results in the following

$$\mathbf{Y}_m = \mathbf{D}_m\mathbf{F}\mathbf{c} + \mathbf{Z} \tag{2.6}$$

where $\mathbf{Y}_m$ is the measurement vector and $\mathbf{D}_m\mathbf{F}$ is the sensing matrix. Precisely it is only the portion where we have reserved carriers.

Consider a system of equations

$$\mathbf{v} = \mathbf{\Phi}\mathbf{c} + \mathbf{Z} \tag{2.7}$$

To formulate the problem the IT algorithm solves, let $\mathbf{v} \in \mathbb{C}^M$ be the measurement vector. We need to find the sparse clipping signal $\mathbf{c}$ given a sensing matrix $\mathbf{\Phi} \in \mathbb{C}^{M \times N}$, with more unknowns than measurements, i.e., $M<N$, such that the error $\|\mathbf{v} - \mathbf{\Phi}\mathbf{c}\|_2<\epsilon$, where ϵ is a small positive number [27].

The IT algorithm works with a thresholding operator H_λ that acts on each element of $\mathbf{c}$ depending on the type of IT algorithm that we are using, i.e., IHT or IST [14]. The main inputs given to the algorithm are: the observed signal, the sensing matrix, the threshold operator, and the dimensionality of the transmitted OFDM signal, i.e. $\mathbf{v}$, $\mathbf{\Phi}$, λ, and N respectively. Comparing (2.6) and (2.7), $\mathbf{v} = \mathbf{Y}_m$ and $\mathbf{\Phi} = \mathbf{D}\mathbf{F}$. As for λ, it is a parameter that is chosen depending on the sparsity level of the unknown signal.

2.3 Iterative Thresholding vs. Iterative Maximum-Likelihood

The algorithm in both cases (IHT and IST) proceeds as the following. Initiates the iterations counter t with the trivial value for $\mathbf{c}_1 = 0$ and perform the thresholding operator for the proceeding iterations as

$$\mathbf{c}_{t+1} = H_\lambda(\mathbf{c}_t + \mathbf{\Phi}^H(\mathbf{v} - \mathbf{\Phi}\mathbf{c}_t)) \tag{2.8}$$

For a vector $\mathbf{w}$, operator $H_\lambda(\mathbf{w})$ will calibrate the elements in $\mathbf{w}$ with the threshold λ, then sets all relatively small elements in $\mathbf{w}$ to zero, in one of the following ways [14]

2.3.1 IHT

$$H_\lambda(\mathbf{w}) = \begin{cases} w & |w| > \sqrt{\lambda} \\ 0 & |w| \leq \sqrt{\lambda} \end{cases} \tag{2.9}$$

2.3.2 IST

$$H_\lambda(\mathbf{w}) = \begin{cases} w + \sqrt{\lambda} & w \leq -\sqrt{\lambda} \\ 0 & |w| < \sqrt{\lambda} \\ w - \sqrt{\lambda} & w \geq \sqrt{\lambda} \end{cases} \tag{2.10}$$

These schemes (IHT and IST) are compared with ItML. ItML is considered one of the most popular nonlinear distortion mitigation technique in literature, used in many works as a benchmark [31]. The algorithm ultimately performs data estimation iteratively by making hard decisions in the frequency domain.

2.4 Enhanced Recovery by Phase-Augmentation and Data-Aided Approach

Up to this point, the IT recovery algorithm is employed in its general setting to recover $\mathbf{c}$. However, our purpose is to enhance the recovery process by including information that is available due to the nature of the overall transmission system $\mathbf{y} = \mathbf{H}\mathbf{x}_p + \mathbf{z}$. It can be seen from (2.4) that $\mathbf{c}$ is linked to $\mathbf{x}_p$ by the fact that it is superimposed on $\mathbf{x}$ in the time domain [31]. The anti-phase relation can be expressed as following [32]

$$\exp(j\angle c(i)) = -\exp(j\angle x_p(i)) \tag{2.11}$$

Given (2.11) we can simplify $\mathbf{c}$ by taking it to polar form to have the clipping signal appear as

$$c(i) = |\hat{c}(i)|(-\exp(j\angle x_p(i))) \tag{2.12}$$

where $\hat{c}(i)$ is the estimate of $\mathbf{c}$ that is found from the IT algorithm. Thus, it is only logical to take advantage of this information to obtain an enhanced estimate of $\mathbf{c}$. Moreover, we also note that the unknown $|\hat{c}(i)|$ that we seek to find represents the magnitude of the unknown clipping signal and hence is a non-negative real value.

Our other objective is to modify the algorithm by using a data-aided method to estimate the measurement vector $\mathbf{v}$ for the sparse model. From (2.6) we notice that $\mathbf{v}$ requires the knowledge of the reserved part of the original signal $\mathbf{X}$ i.e., $\mathbf{X}_m$. However, we know that practically we can not have such knowledge at the receiver's side. So we approach this problem by taking the most reliable elements from $\mathbf{X}_p$. The method of finding the

reliable data is described later in part 2 of this section.

As a result, two features have been added to improve the estimation of the clipping signal **c**. The first feature is that the active coefficients of **c** are anti-phased with the data coefficients, hence we incorporate phase information in the IT algorithm with unknown being the magnitude of the clipping signal **c**. The second feature is replacing pilots from **X** with viable data from the received clipped signal $\mathbf{X}_p$. In this section we will address both features in more detail.

2.4.1 Phase-Augmentation Sparse Model

Since we know that $\angle c(i) = \angle x_p(i) + \pi$, we can incorporate the phase information with the sensing matrix $\mathbf{\Phi}$. From the signal representation in (2.12) let us construct a diagonal matrix $\mathbf{\Theta}$ of size NxN such that the diagonal elements are the phases and zeros off the diagonal. The sparse model can now be written as the following [9], [10]:

$$\mathbf{v} = \mathbf{\Phi} \begin{bmatrix} -e^{j\angle x_p(0)} & \cdots & 0 \\ \vdots & \ddots & \vdots \\ 0 & \cdots & -e^{j\angle x_p(N-1)} \end{bmatrix} \begin{bmatrix} |c(0)| \\ \vdots \\ |c(N-1)| \end{bmatrix} + \mathbf{Z} \tag{2.13}$$

$$\mathbf{v} = \mathbf{\Phi\Theta}(|\mathbf{c}|) + \mathbf{Z} \tag{2.14}$$

Let $\mathbf{\Psi} = \mathbf{\Phi\Theta}$. So the CS algorithm is now fed by a new sensing matrix $\mathbf{\Psi}$, modifying the sparse model to be $\mathbf{v} = \mathbf{\Psi}|\mathbf{c}| + \mathbf{Z}$. Reducing the unknown from a complex signal to a real signal is expected to improve the reconstruction accuracy. All CS algorithms can utilize such additional information about

the unknown. This knowledge allows us to increase the M complex measurements, elements in $\mathbf{v}$, into $2M$ real measurements. That is because the IT algorithm will search for a sparse $\mathbf{c}$ in $\mathbb{R}^N$, instead of $\mathbb{C}^N$. Basically, the search space will be reduced when we apply the measurement vector augmentation. Yielding to the modification of the CS model to be

$$\begin{bmatrix} \Re(\mathbf{v}) \\ \Im(\mathbf{v}) \end{bmatrix} = \begin{bmatrix} \Re(\mathbf{\Psi}) \\ \Im(\mathbf{\Psi}) \end{bmatrix} |\mathbf{c}| + \begin{bmatrix} \Re(\mathbf{Z}) \\ \Im(\mathbf{Z}) \end{bmatrix} \tag{2.15}$$

Therefore, we propose to enforce the positivity constraint in this work. Hence, the IHT and IST will be modified as following

1. IHT

$$H_\lambda(a) = \begin{cases} a & a > \sqrt{\lambda} \\ 0 & a \leq \sqrt{\lambda} \end{cases} \tag{2.16}$$

2. IST

$$H_\lambda(a) = \begin{cases} 0 & a < \sqrt{\lambda} \\ a - \sqrt{\lambda} & a \geq \sqrt{\lambda} \end{cases} \tag{2.17}$$

2.4.2 Data-Aided Approach for Clipping Estimation

Here we use the idea of reliable carriers at the receiver, instead of relying solely on pilot carriers. This allows use to increase the spectral efficiency of the system. Hence, we use reliable carriers from the received clipped signal $\mathbf{X}_p$ to enhance the estimation of $\mathbf{v}$. The scheme used is outlined as following:

1. We estimate the transmitted frequency domain signal $\mathbf{X}_p$ by making the ML decisions, resulting in $\lfloor \hat{\mathbf{X}}_p \rfloor$.

2. Then we construct the reliability metric which is a function of the i^{th} subcarrier as following $\mathfrak{R}(\mathfrak{i}) = |\lfloor \hat{X}_p(i) \rfloor - X_p(i)|$. We measure the reliability of all subcarriers. The higher the value of $\mathfrak{R}$ the less probability of staying in the correct decision region and hence the less reliability of the subcarrier. Therefore, we ascend the vector $\mathfrak{R}$ and choose the first M number of measurements as our reliable data.

3. Use the R reliable carriers instead of pilots to represent the signal $\mathbf{X}_p^R$.

2.5 Multiple Antenna Base-station

In this section, we look at the case of multiple receiving antennas on the BS i.e., a SIMO setup. So each antenna will receive the same clipped signal but transmitted through different channels. Hence, the received clipped signal may vary among different antennas. So for an A antenna system, we will have A equations of the form (2.7). Thus we have

$$\begin{aligned} \mathbf{v}_1 &= \mathbf{\Phi}_1 \mathbf{c} + \mathbf{Z}_1 \\ \mathbf{v}_2 &= \mathbf{\Phi}_2 \mathbf{c} + \mathbf{Z}_2 \\ &\vdots \\ \mathbf{v}_A &= \mathbf{\Phi}_A \mathbf{c} + \mathbf{Z}_A \end{aligned} \tag{2.18}$$

where $\mathbf{v}_A$, $\mathbf{\Phi}_A$, and $\mathbf{c}$ represent the measurement vector, sensing matrix, and the unknown clipping signal of the A^{th} antenna respectively. The IT algorithm then takes the combined measurement vectors and combined sensing matrices as inputs after applying the phase augmentation. That way the

algorithm allows us to increase the number of measurements by A times. We also use the SIMO setup with the data-aided case by having each antenna find its own reliable carriers from their received signal to find the measurement vector.

2.6 Simulation Results

For simulation purposes we used the OFDM system with $N = 512$ subcarriers. The data coefficients were generated from a QAM constellation of order $Q = 64$. The channel length was selected to be $L = N/4$, which makes the channel a 128 tap Rayleigh fading channel, in which each tap comes from standard normal distribution and results are averaged over $9\text{x}10^3$ bit errors. The CR = 1.54. The λ for the IT algorithm was chosen to be $\lambda = 0.4$, this value is numerically optimized for best performance. The stopping condition used for the IT algorithm is number of iterations $t = 200$. The number of reliable tones selected is $R = 200$ and the number of reserved tones (pilots) used is $m = 100$. As for the ItML the number of iterations used is $q = 10$. In the case of multi-antenna base-station we use $A = 2$ antennas.

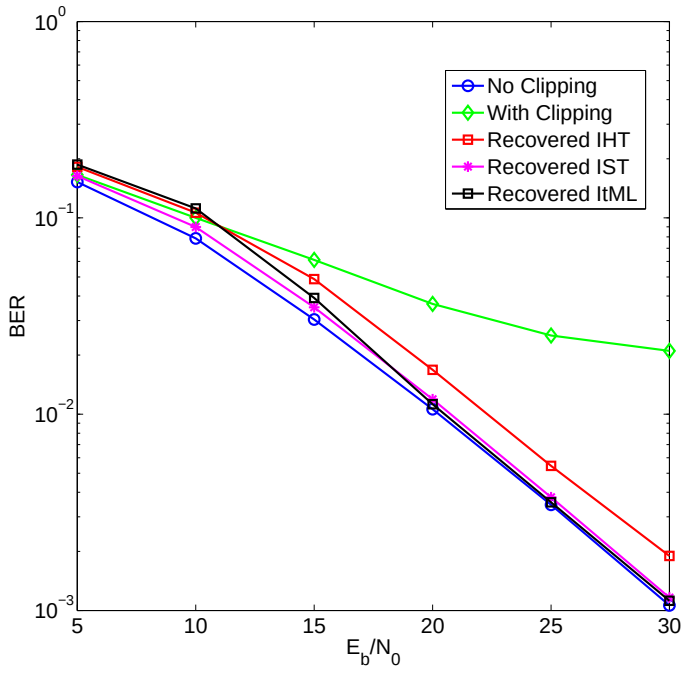

Figure 2.1: BER performance of the IST and IHT algorithms using reserved carriers as a function of E_b/N_0.

Figure 2.1 illustrates the BER performance of the algorithms using reserved carriers recovery against different E_b/N_0 values. As it appears the IST recovery performs better than ItML at lower E_b/N_0 values and almost similar performance to ItML at higher values of E_b/N_0. However, IHT recovery has a performance that is comparable with ItML at lower values of E_b/N_0 then towards higher values of E_b/N_0 both ItML and IST outperform IHT.

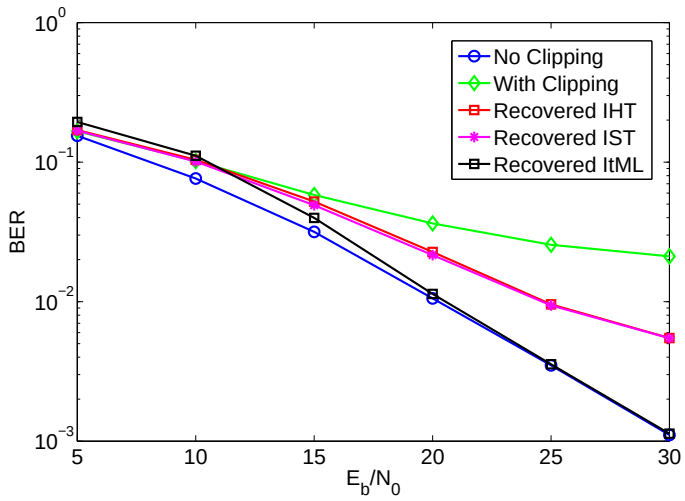

Figure 2.2: BER performance of the IST and IHT data-aided algorithms as a function of E_b/N_0.

In figure 2.2, we show the results of IST and IHT recovery using the data-aided approach i.e., using reliable carriers for recovery. We notice that both IST and IHT have very similar performance throughout the range of E_b/N_0. As we move towards higher values of E_b/N_0 the impact of the clipping signal recovery on the BER performance of the system starts to become more pronounced.

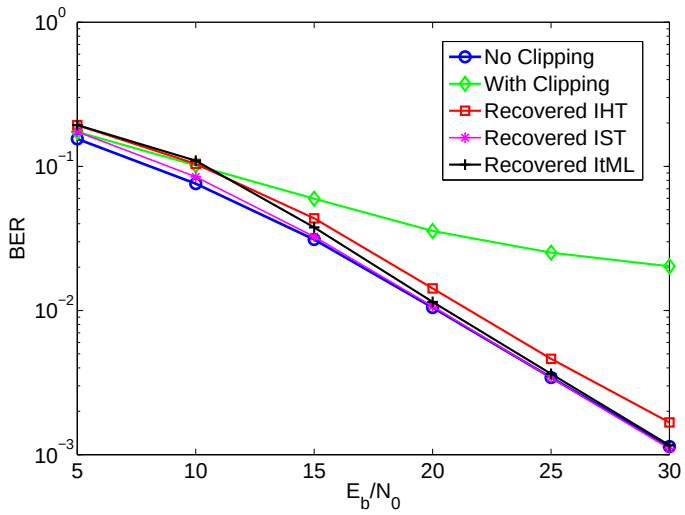

Figure 2.3: BER performance of the IST and IHT algorithms using reserved carriers as a function of E_b/N_0 in the SIMO scenario.

Figure 2.3 demonstrates the results of IST and IHT in the SIMO setup with the use of reserved tones only. As observed, the results show better performance than that in the single receiver case. IST is seen to outperform ItML throughout all values of the E_b/N_0 range. ItML has lower BER than IHT, however IHT in this case shows an enhanced performance than the IHT performance in figure 1.

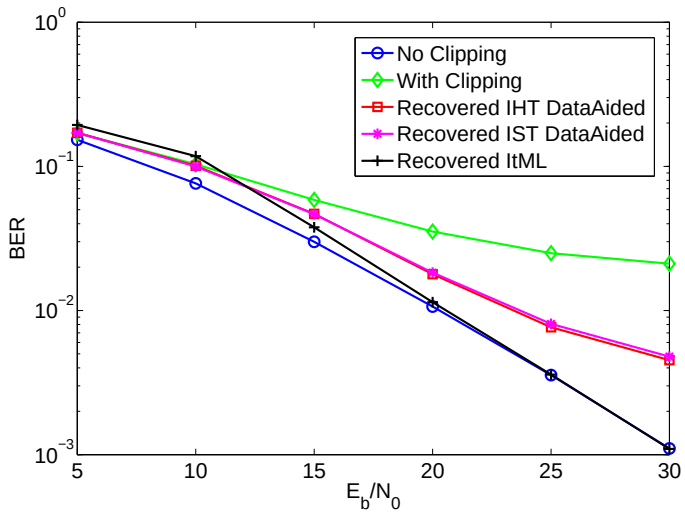

Figure 2.4: BER performance of the IST and IHT data-aided algorithms as a function of E_b/N_0 in the SIMO scenario.

In figure 2.4, it shows the data-aided approach in the SIMO system. As in the data-aided single receiver case, both IHT and IST have very close performances. Here, however, the recovery of the data-aided IT algorithms show improvement in the BER performance than the case of single receiver.

2.7 Conclusion

A low complexity CS technique has been proposed for PAPR reduction in an OFDM system. The IT algorithm with its both types i.e., IST and IHT, incorporate phase-augmentation to further enhance the recovery performance.

The IST algorithm was found to perform better in terms of BER than the IHT algorithm in all the cases studied. In comparison with ItML, IST was found to have very similar performance to it in the case of reserved tones. Furthermore, a data-aided approach was used to rely on reliable carriers instead of reserved tones, which are much feasible and applicable. It was found that the recovery of IT data-aided is reasonably effective, knowing the fact that the spectral efficiency of the system is further enhanced. The OFDM system is then upgraded to a SIMO scenario where measurements are increased leading the CS technique to have more data to take advantage of for recovery. The IT algorithms in the SIMO case show improved performance than the single receiver case.

Chapter 3

Clipping Distortion Mitigation in Clipped OFDMA Systems

3.1 Introduction

In the second chapter, we proposed clipping at the transmitter and iterative thresholding based compressed sensing recovery at the receiver as a solution to high PAPR problem in OFDM signals. In this chapter, we extend the compressed sensing based clipping recovery approach to OFDMA systems. OFDMA is a multi-user system that allows high-data-rate transmissions over wireless channels by sharing the frequency resources among multiple users [33]. However, like OFDM, OFDMA suffers from high PAPR. In this chapter, we discuss the problem of clipping mitigation in OFDMA, and outline conditions under which the clipping recovery scheme proposed in chapter two, can be conveniently extended to OFDMA systems.

Unlike clipping in the single user scenario, when multi-users are clipped at

their respective transmitters, the clipping distortions from all users overlap in the frequency domain [30]. As the measurements of compressed sensing based clipping recovery are taken in frequency domain, this distortion overlap has a dire impact on the reliability of the measurements. However, it is observed that interleaved OFDMA(i.e., OFDMA setup where the subcarrier allocation is interleaved), clipping distortions are only self-inflicted, i.e., the clipping distortions from user u are confined only to the subcarriers that are allocated to the user u itself. This, however, is not true for consecutive carrier allocation, where distortion overlap is a serious issue from CS based clipping recovery viewpoint [30].

In this chapter, we present a mathematical proof authenticating the observation that clipping distortions are self inflicted for interleaved OFDMA. We start by introducing the data model for a clipped OFDMA system. Then we explain the proposed solution to clipping distortion mitigation. We proceed by providing a mathematical proof of the solution. We then present the CS recovery model. Finally, we illustrate the simulation results.

3.2 Data Model

In the second chapter, we explained the OFDM model as an N dimensional data vector $\mathbf{X} = [X(0), X(1), ..., X(N-1)]^\top$ that results after mapping the N parallel streams to an M-ary QAM. We find the time domain signal vector $\mathbf{x}$ by applying an N dimensional IDFT $\mathbf{F}^H$, so that $\mathbf{x} = \mathbf{F}^H\mathbf{X}$.

In a U user OFDMA system, each user is assigned a total of P sub-carriers (where $P = N/U$) and each sub-carrier is assigned to one user only. The

P dimensional data vector $\mathbf{X}^u$ is then mapped to the allocated subcarriers using a resource allocation matrix $\mathbf{M}^u$ of size $N \times P$. We can define $\mathbf{M}^u$ as a partial identity matrix of size $N \times P$ with the selected columns being the corresponding locations of the subcarriers designated to user u. Now the time domain data from user u can be written as

$$\mathbf{x}^u = \mathbf{F}^H \mathbf{M}^u \mathbf{X}^u \tag{3.1}$$

where $\mathbf{M}^u\mathbf{X}^u$ is the N dimensional data vector with non-zero values only at locations of the subcarriers allocated for the u^{th} user. To reduce the PAPR in $\mathbf{x}^u$, the signal is subjected to clipping. The clipping operation limits the maximum amplitude to the threshold γ^u [29]. The clipping operation can be mathematically written as [30]:

$$x_c^u(n) = \begin{cases} \gamma^u e^{j\angle x^u(n)} & \text{if } \mid x^u(n) \mid > \gamma^u \\ x^u(n) & \text{otherwise} \end{cases} \tag{3.2}$$

where $x_c^u(n)$ is the n^{th} element of the u^{th} signal $\mathbf{x}^u$ after clipping, and $\angle x^u(n)$ is the phase of the original signal $x^u(n)$. The clipping threshold γ^u is related to the CR as $\text{CR}^u = \gamma^u/\sigma^u$ [30], where σ^u is the root mean squared power of the OFDM signal transmitted by the u^{th} user.

This results in the following expression:

$$\mathbf{x}_c^u = \mathbf{x}^u + \mathbf{c}^u \tag{3.3}$$

where $\mathbf{c}^u$ is the clipping signal from the u^{th} user. The clipping signal $c^u(n)$ is anti-phased with $x^u(n)$ on the clipping locations.

The clipped signal $\mathbf{x}_c^u$ is then transmitted through a channel of length N_c with impulse response $\mathbf{h}^u = [h^u(0), h^u(1), ..., h^u(N_c - 1)]^\top$. Hence, the received time domain signal can be expressed as $\mathbf{y}^u = \mathbf{H}^u\mathbf{x}_c^u$, where $\mathbf{H}^u$ is the circulant channel matrix which can be diagonalized using the DFT matrix $\mathbf{F}_{N\times N}$ and can be expressed as $\mathbf{H}^u = \mathbf{F}^H\mathbf{D}^u\mathbf{F}$. Where $\mathbf{D}^u$ is a diagonal matrix with the partial Fourier transform of the impulse response of the u^{th} user i.e., $\bar{\mathbf{F}}\mathbf{h}^u$ on its diagonal. The received time domain signal at the base station can be written as

$$\mathbf{y} = \sum_{u=0}^{U-1} \mathbf{H}^u(\mathbf{x}^u + \mathbf{c}^u) + \mathbf{z} \tag{3.4}$$

where $\mathbf{y}$ is the combined channel output of all users plus additive white Gaussian noise (AWGN), $\mathbf{z} \sim \mathcal{N}(0, \sigma_z^2\mathbf{I}_N)$.

The frequency domain received signal can be obtained by the DFT operation as following

$$\mathbf{Y} = \sum_{u=0}^{U-1} \mathbf{D}^u\mathbf{M}^u\mathbf{X}^u + \sum_{u=0}^{U-1} \mathbf{D}^u\mathbf{M}^u\mathbf{C}^u + \mathbf{Z} \tag{3.5}$$

where the frequency domain white Gaussian vector $\mathbf{Z}$ has the same statistics as $\mathbf{z}$. The column vector resulting from $\mathbf{D}^u\mathbf{M}^u\mathbf{X}^u$ at each user u will have non-zero values only at locations corresponding to the sub-carriers allocated to the u^{th} user.

3.3 Special Case: Interleaved OFDMA

With interleaved allocation, subcarriers are allocated to each user in turn. In the case of an OFDMA signal with N subcarriers, U users, and $P = N/U$

subcarriers per user, the $(k,l)^{th}$ element of the resource allocation matrix $\mathbf{M}^u$ is given by

$$m^u(k,l) = \begin{cases} 1, & k = u + Ul, \qquad 0 \leq l \leq P-1 \\ 0, & \text{otherwise} \end{cases} \tag{3.6}$$

At this stage, we conjecture that for the interleaved subcarrier assignment the clipping distortion is only self-inflected, i.e., when the clipping distortions from the user u are viewed in frequency domain, they only fall on the subcarriers allocated to user u. The clipping vector in the frequency domain i.e., $\mathbf{M}^u\mathbf{C}^u$ looks like

$$\mathbf{M}^u\mathbf{C}^u = \begin{bmatrix} \mathbf{0}_u & C^u(0) & \mathbf{0}_{U-1} & C^u(1) & \dots & C^u(P-1) & \mathbf{0}_{U-(u+1)} \end{bmatrix}^\top \tag{3.7}$$

where $\mathbf{0}_u$ is the zero vector of length u and $C^u(p)$ is the p^{th} element of the u^{th} user in the clipping signal. Figure 3.1 illustrates the clipping signal of the 0^{th} user when $N = 64$ and the overall number of users is $U = 8$. As observed, the clipping distortion only occurs at the subcarriers allocated for user 0.

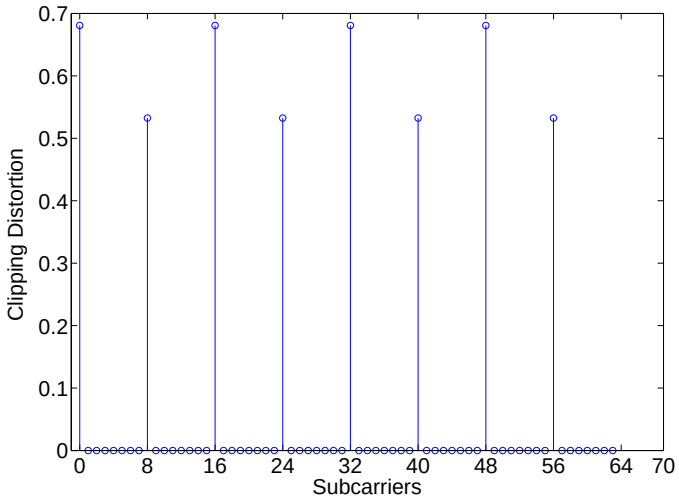

Figure 3.1: The clipping distortions of the 0^{th} user.

In the following subsection we outline the mathematical proof that shows that (3.7) is always true.

3.3.1 Proof of Self-Inflected Clipping Distortion in Interleaved OFDMA

To start the proof, we first show the data generated and allocated for user u. For simplicity we will show when the 0^{th} user is subjected to clipping i.e., $u = 0$, the allocated data will look like the following

$$\mathbf{M}^0\mathbf{X}^0 = \begin{bmatrix} f^0(0) & \mathbf{0}_{U-1} & f^0(1) & \dots & f^0(P-1) & \mathbf{0}_{U-1} \end{bmatrix}^\top \tag{3.8}$$

where $f^0(p)$ is the p^{th} element of the 0^{th} user's data in the frequency domain.

Since data is clipped in the time domain, the result from (3.8) is multipied by the IDFT matrix $\mathbf{F}^H$ as following

$$
\begin{aligned}
& \mathbf{F}^H \begin{bmatrix} f^0(0) & \mathbf{0}_{U-1} & f^0(1) & \dots & f^0(P-1) & \mathbf{0}_{U-1} \end{bmatrix}^\top \\
= \; & \frac{1}{\sqrt{N}} \begin{bmatrix} f^0(0)e^{j\frac{2\pi}{N}(0)(0)} + f^0(1)e^{j\frac{2\pi}{N}(0)(U)} + \ldots + f^0(P-1)e^{j\frac{2\pi}{N}(0)(P-1)(U)} \\ f^0(0)e^{j\frac{2\pi}{N}(1)(0)} + f^0(1)e^{j\frac{2\pi}{N}(1)(U)} + \ldots + f^0(P-1)e^{j\frac{2\pi}{N}(1)(P-1)(U)} \\ \vdots \\ f^0(0)e^{j\frac{2\pi}{N}(N-1)(0)} + f^0(1)e^{j\frac{2\pi}{N}(N-1)(U)} + \ldots + f^0(P-1)e^{j\frac{2\pi}{N}(N-1)(P-1)(U)} \end{bmatrix} \\
= \; & \begin{bmatrix} t^0(0) \\ t^0(1) \\ \vdots \\ t^0(N-1) \end{bmatrix}
\end{aligned}
\tag{3.9}
$$

where $t^0(n)$ is the n^{th} element of the 0^{th} user's data in the time domain. It is noted that the time domain signal found in (3.9) is periodic with period P, i.e., N/U. To prove that, let us show that $t^0(r) = t^0(r+P)$ where r could be any row that satisfies $0 \leq r \leq P-1$. The proof proceeds as following

$$
\frac{1}{\sqrt{N}}(f^0(0)e^{j\frac{2\pi}{N}(r)(0)} + f^0(1)e^{j\frac{2\pi}{N}(r)(U)} + \ldots + f^0(P-1)e^{j\frac{2\pi}{N}(r)(P-1)(U)}) \tag{3.10}
$$

$$
\Updownarrow
$$

$$
\frac{1}{\sqrt{N}}(f^0(0)e^{j\frac{2\pi}{N}(r+P)(0)} + f^0(1)e^{j\frac{2\pi}{N}(r+P)(U)} + \ldots + f^0(P-1)e^{j\frac{2\pi}{N}(r+P)(P-1)(U)}) \tag{3.11}
$$

Let us deal with the problem term wise and show that the first terms of (3.10) and (3.11) are equal. To establish that, we simplify the terms even more yielding

$$f^0(0)e^{j\frac{2\pi}{N}(r)(0)} = f^0(0) \times 1 = f^0(0) \tag{3.12}$$

from (3.10) and

$$f^0(0)e^{j\frac{2\pi}{N}(r+P)(0)} = f^0(0) \times 1 = f^0(0) \tag{3.13}$$

from (3.11). Hence, from (3.12) and (3.13) we see that the terms are indeed equal.

We proceed by proving the second terms of (3.10) and (3.11) are equal as well. This will result in the following (note that $U = N/P$ and $(e^{j2\pi})^K = 1$ where K is an integer)

$$f^0(1)e^{j\frac{2\pi}{N}(r)(U)} \tag{3.14}$$

from (3.10) and

$$\begin{aligned} f^0(1)e^{j\frac{2\pi}{N}(r+P)(U)} &= f^0(1) \times e^{j\frac{2\pi}{N}(rU+PU)} = f^0(1) \times e^{j\frac{2\pi}{N}(rU)} \times e^{j\frac{2\pi}{N}(PU)} \\ &= f^0(1) \times e^{j\frac{2\pi}{N}(rU)} \times e^{j\frac{2\pi}{N}(P\frac{N}{P})} = f^0(1) \times e^{j\frac{2\pi}{N}(rU)} \times e^{j2\pi} \\ &= f^0(1) \times e^{j\frac{2\pi}{N}(rU)} \times 1 = f^0(1)e^{j\frac{2\pi}{N}(rU)} \end{aligned} \tag{3.15}$$

from (3.11). Hence, from (3.14) and (3.15) we see that the second terms are also equal.

The process of proving the equality of the terms goes on until we reach the last terms. Here, we show the proof of equality for the last term of (3.10) and (3.11),

$$f^0(P-1)e^{j\frac{2\pi}{N}(r)(P-1)(U)} \tag{3.16}$$

from (3.10) and

$$f^0(P-1)e^{j\frac{2\pi}{N}(r+P)(P-1)(U)} = f^0(P-1) \times e^{j\frac{2\pi}{N}(r)(P-1)(U)} \times e^{j\frac{2\pi}{N}(P)(P-1)(\frac{N}{P})}$$

$$= f^0(P-1) \times e^{j\frac{2\pi}{N}(r)(P-1)(U)} \times (e^{j2\pi})^{(P-1)} = f^0(P-1) \times e^{j\frac{2\pi}{N}(r)(P-1)(U)} \times 1$$

$$= f^0(P-1)e^{j\frac{2\pi}{N}(r)(P-1)(U)} \tag{3.17}$$

from (3.11). Hence, from (3.16) and (3.17) we see that the final terms are also equal.

As a result, the time domain signal from (3.9) for any user is indeed periodic for period P. The signal in (3.9) now goes through the clipping process leading to a clipping signal $\mathbf{c}^u$ that is periodic for period P as well, (note that for consistency reasons we keep operating with the 0^{th} user, however the same approach may work for any u user)

$$\mathbf{c}^0 = \begin{bmatrix} c^0(0) \\ c^0(1) \\ \vdots \\ c^0(N-1) \end{bmatrix} \tag{3.18}$$

To prove the self-inflicted clipping distortion of the 0^{th} user, we transform (3.18) to frequency domain using the DFT matrix $\mathbf{F}$. A property of the Fourier matrix, when transforming a time domain periodic signal, the

product has non-zero values only at locations of the harmonics of U i.e., $0, \pm U, \pm 2U, \ldots$, otherwise the value is zero. Hence, the resulting frequency domain clipping signal for the 0^{th} user will look as following

$$\mathbf{M}^0\mathbf{C}^0 = \begin{bmatrix} C^0(0) & \mathbf{0}_{U-1} & C^0(1) & \ldots & C^0(P-1) & \mathbf{0}_{U-1} \end{bmatrix} \top \tag{3.19}$$

A general way to write (3.19) for any user u clipped is as in (3.7).

3.4 Compressive Sensing Recovery Model

Now that we have proved that the clipping distortions from different users do not spread or overlap between different users, we seek to recover the clipping signal $\mathbf{M}^u\mathbf{C}^u$ at the receiver's side. To do that we show the recovery model used to reconstruct the original signal $\mathbf{M}^u\mathbf{X}^u$. Knowing that the data is allocated in an interleaved manner, the CS model can be constructed from (3.5). Taking into account that the recovery process works with each user individually in (3.5) i.e., selecting the entries in $\mathbf{Y}$ and $\mathbf{Z}$ that correspond to the subcarriers allocated to user u, resulting in the following

$$\mathbf{Y}^u = \mathbf{D}^u\mathbf{M}^u\mathbf{X}^u + \mathbf{D}^u\mathbf{M}^u\mathbf{C}^u + \mathbf{Z}^u \tag{3.20}$$

We further extend (3.20) to an equation with sparse unknown we start with $\mathbf{Y}^u - \mathbf{D}^u\mathbf{M}^u\mathbf{X}^u = \mathbf{D}^u\mathbf{M}^u\mathbf{C}^u + \mathbf{Z}^u$. By reserving some carriers to sense clipping from user u, we are able to get the measurement vector for the model. The number of reserved tones is said to be s. The same goes to $\mathbf{D}^u$, the matrix will only have the rows corresponding to those reserved tones, changing the size of $\mathbf{D}^u$ to be $s \times N$. Hence, we get

$$\mathbf{Y}_s^u = \mathbf{D}_s^u \mathbf{M}^u \mathbf{C}^u + \mathbf{Z}_s^u \tag{3.21}$$

where $\mathbf{Y}_s^u$ and $\mathbf{Z}_s^u$ are of size $s \times 1$.

Since our sparse unknown is $\mathbf{c}^u$, we can transform $\mathbf{M}^u\mathbf{C}^u$ to $\mathbf{c}^u$ by using the DFT matrix as $\mathbf{M}^u\mathbf{C}^u = \mathbf{F}\mathbf{c}^u$. This results in the following

$$\mathbf{Y}_s^u = \mathbf{D}_s^u \mathbf{F} \mathbf{c}^u + \mathbf{Z}^u \tag{3.22}$$

where $\mathbf{Y}_s^u$, $\mathbf{D}_s^u\mathbf{F}$, and $\mathbf{c}^u$ are the measurement vector, the sensing matrix, and the unknown sparse signal respectively.

3.5 Simulation Results

An OFDMA system with $N = 128$ subcarriers is simulated, with $U = 2$ active users accessing the frequency resources. The data is modulated using a QAM constellation of order $Q = 64$. The channel length is $N_c = \frac{N}{4}$.

As observed from figure 3.2, the FBMP [17] is successfully recovering the original signal back due to the absence of clipping distortions spreading from different users. The CR selected in figure 2 is $\sqrt{3}$ and the number of reserved tones used is $s = 32$.

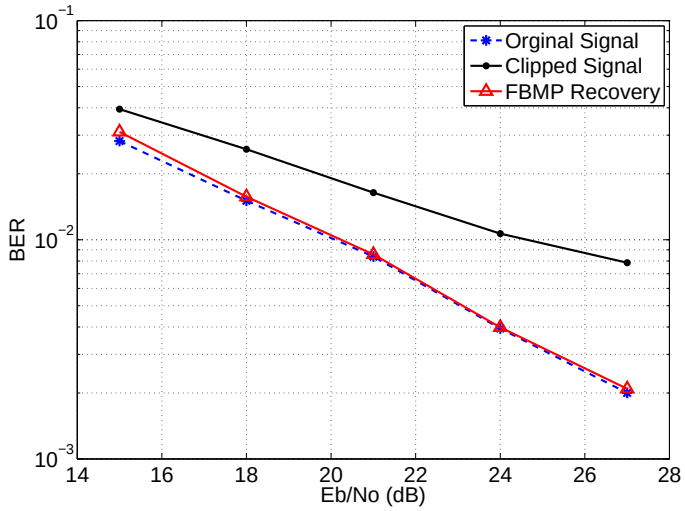

Figure 3.2: BER performance of the FBMP recovery scheme as a function of E_b/N_0 (interleaved carrier assignment).

In figure 3.3, we see the result of FBMP recovery when subcarriers are assigned in a non-interleaving manner, i.e., consecutive assignment. As observed, the recovery performance is very poor due to overlapping clipping distortions from both users.

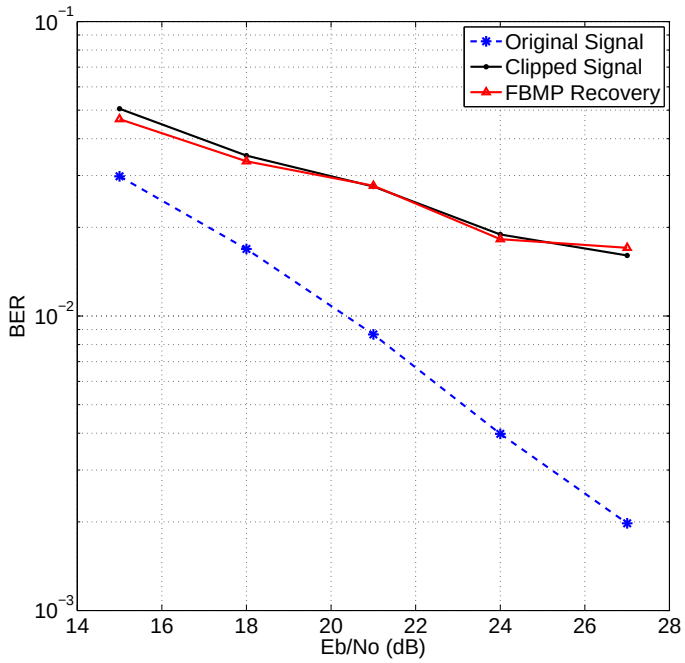

Figure 3.3: BER performance of the FBMP recovery scheme as a function of E_b/N_0 (consecutive carrier assignment).

In figure 3.4, the number of reserved tones are varying where E_b/N_0 is fixed to 20 dB and CR= $\sqrt{3}$. We notice that the more reserved carriers there are, the better the performance of the FBMP recovery gets and this is what we expect. That is because it leads to an increase in the measurement vector used in CS model, which results in a better estimation of the original signal.

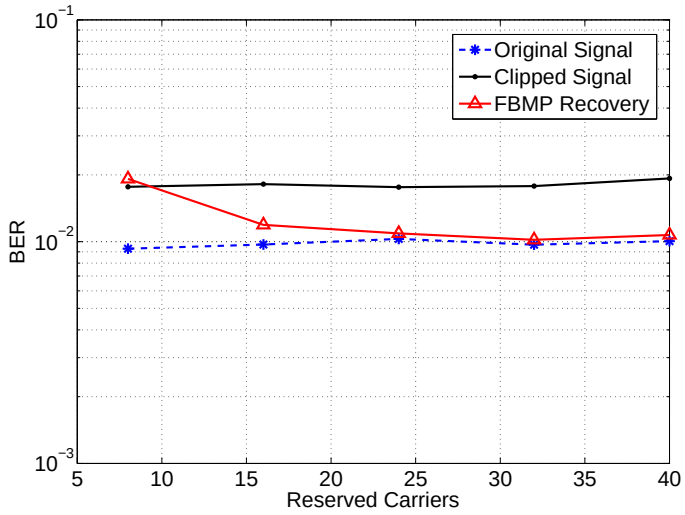

Figure 3.4: BER performance of the FBMP recovery scheme as a function of reserved carriers s (interleaved carrier assignment).

In figure 3.5, we vary the CR and keep E_b/N_0 fixed at 20 dB and reserved pilots fixed at $s = 32$. From the definition of CR in the data model, we see that it has a proportional relationship with the clipping threshold γ^u. So as observed we notice as CR increases (i.e., clipping threshold increases) the recovery signal tends to be closer to the original signal, which means that not much of the original signal is being clipped due to the high threshold. We can see that from the clipped signal as well, the higher the CR the closer it gets to the original signal.

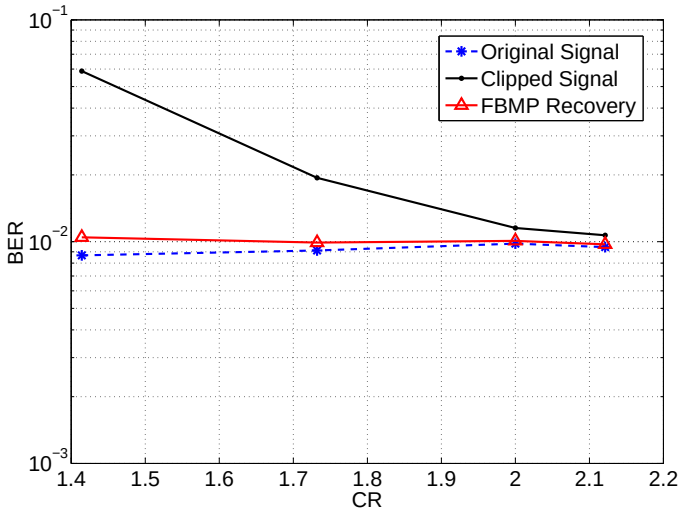

Figure 3.5: BER performance of the FBMP recovery scheme as a function of CR (interleaved carrier assignment).

3.6 Conclusion

The problem of high PAPR in OFDMA signals can be simply solved using the clipping operation. However, in the case of OFDMA, clipping distortions from different users tend to spread and cause disruption to other users in the frequency domain. This makes compressed sensing based clipping recovery unfeasible. To solve this problem, we proved that for the case of interleaved OFDMA, the clipping signal is purely self inflicted and hence it is straightforward to utilize FBMP for its recovery, once a suitable CS system is formed.

Our numerical findings are also aligned with theoretical observations and illustrate that simple CS recovery is sufficient for interleaved OFDMA.

Chapter 4

Narrowband Interference Cancellation in SC-FDMA Systems

4.1 Introduction

In the second chapter we highlighted the main disadvantage of using OFDM i.e., high PAPR. We clipped at the transmitter to reduce the PAPR and used IT to recover the clipped data. We also extended the proposed clipping based PAPR reduction method to OFDMA systems in chapter three. However, an alternative approach to reduce the PAPR is the complete redesign of the transmission waveform. As such a modified OFDMA scheme i.e., SC-FDMA was proposed. SC-FDMA is widely used in uplink transmission and is employed in the long term evolution [8] ,[4].

SC-FDMA retains the advantages of OFDMA and compliments them

with lower PAPR. However, like any wideband scheme, SC-FDMA is highly susceptible to NBI. An OFDMA system is also equally susceptible to NBI, however, the impact of NBI on SC-FDMA system is more pronounced. This is due to the fact that the data in SC-FDMA system is transmitted in time domain and hence even a single NBI source affects all the data. In contrast the data in OFDMA is encoded in the frequency domain and hence a single NBI source corrupts data only on one tone and leaves the rest of the data unimpaired [8]. Therefore, the process of NBI cancellation in SC-FDMA is important to achieve reliable communication.

In this work, we take advantage of the sparse nature of the NBI signal to recover it using the SABMP algorithm proposed in [16]. Further, we employ a data-aided approach that allows us to use less reserved tones to increase the system spectral efficiency. We further extend the recovery scheme to a SIMO system by utilizing the fact that the NBI on each receiver antenna shares a common support, but possibly different magnitudes. We then combine the data-aided approach with the SIMO system and finally illustrate the results of the simulations.

4.2 System Model

Consider an SC-FDMA system with U users. In such a system the u^{th} user converts the incoming high rate bit stream into P parallel streams. These P streams go through a M-QAM modulation process which results in a P dimensional data vector $\mathbf{x}_u$. The data in $\mathbf{x}_u$ goes through the process of PAPR reduction by adding an extra step which is Fourier pre-coding using

the $P \times P$ discrete Fourier matrix $\mathbf{F}_P$. The $(k,l)^{th}$ element of $\mathbf{F}_P$ is given by

$$f_p(k,l) = P^{-\frac{1}{2}} \exp(-j\frac{2\pi kl}{P}), \qquad k,l \in 0,1,...,P-1 \tag{4.1}$$

The pre-coded data $\mathbf{F}_P\mathbf{x}_u$ is then mapped to the sub-carriers allocated for the u^{th} user in an interleaved manner. We use interleaved carrier assignment because it is robust to frequency selective fading [8], [4]. By using a resource allocation matrix $\mathbf{M}_u$ of size $N \times P$ the data $\mathbf{F}_P\mathbf{x}_u$ is mapped to the sub-carriers dedicated for user u. The $(k,l)^{th}$ element of $\mathbf{M}_u$ is given by

$$m_u(k,l) = \begin{cases} 1, & k = u + Ul, \qquad 0 \leq l \leq P-1 \\ 0, & \text{otherwise} \end{cases} \tag{4.2}$$

This renders the resource allocation matrices belonging to different users othronormal, i.e.,

$$\mathbf{M}_i^{\mathrm{H}}\mathbf{M}_j = \begin{cases} \mathbf{I}_P, & i = j \\ \mathbf{0}_P, & i \neq j \end{cases} \tag{4.3}$$

Now the pre-coded and resource-allocated data is $\mathbf{X}_u = \mathbf{M}_u\mathbf{F}_u\mathbf{x}_u$ which is in frequency domain. Hence, we perform the IDFT on $\mathbf{X}_u$ to find the desired time domain transmission signal. The time domain signal is then transmitted through a finite impulse response channel of length N_c, $\mathbf{h}_u = [h_u^*(0), h_u^*(1), ..., h_u^*(N_c-1)]^{\mathrm{H}}$. So the received time domain signal (with no NBI) can be expressed as

$$\mathbf{y} = \sum_{u=0}^{U-1} \mathbf{H}_u\mathbf{F}_N^{\mathrm{H}}\mathbf{X}_u + \mathbf{z}, \tag{4.4}$$

where $\mathbf{H}_u$ is the circulant channel matrix for the u^{th} user and $\mathbf{z}$ is the AWGN, $\mathbf{z} \sim \mathcal{CN}(0, \sigma_z^2 \mathbf{I}_N)$. Since $\mathbf{H}_u$ has a circulant nature, this enables us to diagonalize it using the DFT matrix $\mathbf{F}_N$ as $\mathbf{H}_u = \mathbf{F}_N^{\mathrm{H}} \mathbf{\Lambda}_u \mathbf{F}_N$. Here we assume the channel impulse response to be known at the receiver's side. Therefore, $\mathbf{H}_u$ and $\mathbf{\Lambda}_u$ are available. Now we can express the received frequency domain signal

$$\mathbf{Y} = \mathbf{F}_N \mathbf{y} = \sum_{u=0}^{U-1} \mathbf{\Lambda}_u \mathbf{X}_u + \mathbf{Z}, \tag{4.5}$$

where $\mathbf{\Lambda}_u = \mathbf{F}_N \mathbf{H}_u \mathbf{F}_N^{\mathrm{H}}$ and $\mathbf{Z} = \mathbf{F}_N \mathbf{z}$. Taking into consideration the diagonal nature of $\mathbf{\Lambda}_u$ and utilizing (4.3), the data vector $\mathbf{x}_u$ can be estimated by using the ZF-FDE or the MMSE-FDE. However, it is noted that the MMSE-FDE works better in the case when the frequency response contains null as oppose to ZF-FDE. ZF-FDE may cause a dramatic increase in the BER that is caused by the enhancement of the noise [34]-[36]. So we use MMSE-FDE to obtain the following estimate

$$\hat{\mathbf{x}}_{u,\mathrm{MMSE}} = \mathbf{R}_x \mathbf{A}^{\mathrm{H}} (\mathbf{A} \mathbf{R}_x \mathbf{A}^{\mathrm{H}} + \sigma_z^2 \mathbf{I})^{-1} \mathbf{M}_u^{\mathrm{H}} \mathbf{Y}, \tag{4.6}$$

where $\mathbf{R}_x \triangleq \mathbb{E}[\mathbf{x}_u \mathbf{x}_u^{\mathrm{H}}] = \sigma_x^2 \mathbf{I}$ is the auto-correlation matrix of the data vector and $\mathbf{A} \triangleq \mathbf{M}_u^{\mathrm{H}} \mathbf{\Lambda}_u \mathbf{M}_u \mathbf{F}_P$. Since MMSE estimator is linear in $\mathbf{Y}$, we can write $\hat{\mathbf{x}}_u = \mathbf{E}_u \mathbf{Y}$ where

$$\mathbf{E}_u = \sigma_x^2 \mathbf{A}^{\mathrm{H}} (\sigma_x^2 \mathbf{A} \mathbf{A}^{\mathrm{H}} + \sigma_z^2 \mathbf{I})^{-1} \mathbf{M}_u^{\mathrm{H}}, \tag{4.7}$$

Using (4.7), now we can write that $\hat{\mathbf{x}}_u = \mathbf{x}_u + \mathbf{E}_u \mathbf{Z}$, which is approximately true as $\mathbf{E}_u \mathbf{\Lambda}_u \mathbf{M}_u \mathbf{F}_P \approx \mathbf{I}$. This approximation tends to equality as $\sigma_z^2 \to 0$.

Although (4.6) gives a good estimate of $\mathbf{x}_u$ for NBI free signal, it is not suitable for systems experiencing NBI [8]. The following subsection explains the case of NBI impaired SC-FDMA system.

4.2.1 SC-FDMA System NBI Impaired

When the SC-FDMA signal is received it might be affected by a single or multiple time-variant NBI sources [8]. Assume there are L active NBI sources represented using an L dimensional vector $\boldsymbol{\mathcal{I}}_L$. We can obtain an N dimensional NBI signal by using $\boldsymbol{\mathcal{I}}_L$ in the following operation $\boldsymbol{\mathcal{I}} = \mathbf{F}_N \bar{\mathbf{F}}_N^H \boldsymbol{\mathcal{I}}_L$, where $\bar{\mathbf{F}}_N^H$ is $N \times L$ partial IDFT matrix where the columns correspond to the frequencies of the active NBI sources. Note that, the channels between the NBI sources and the BS are absorbed into $\boldsymbol{\mathcal{I}}_L$. Therefore, $\boldsymbol{\mathcal{I}}$ can be simply added to (4.5) to find the received SC-FDMA NBI impaired signal, which can be expressed as following

$$\mathbf{Y} = \sum_{u=0}^{U-1} \boldsymbol{\Lambda}_u \mathbf{X}_u + \boldsymbol{\mathcal{I}} + \mathbf{Z}, \tag{4.8}$$

If it were not for the NBI, (4.6) could be used to obtain an acceptable estimate of $\mathbf{x}_u$. However, now in the case of NBI impaired signal if we follow the same estimation process it will yield

$$\hat{\mathbf{x}}_u = \mathbf{x}_u + \mathbf{E}_u(\boldsymbol{\mathcal{I}} + \mathbf{Z}), \tag{4.9}$$

Because of the presence of $\boldsymbol{\mathcal{I}}$, the estimation of $\mathbf{x}_u$ is not reliable. It is also noted that $\boldsymbol{\mathcal{I}}$ distorts $\mathbf{x}_u$ through the IDFT operation (observed in the construction of $\mathbf{E}_u$), therefore, all data points are perturbed by the NBI

even when we have a single active NBI source. This implies that we must find the value of $\boldsymbol{\mathcal{I}}$ to cancel out its effect in the signal. In the following section we explain the Bayesian sparse recovery algorithm that we will use for estimation and mitigation of the NBI.

4.3 Bayesian Sparse Recovery of the NBI

To reconstruct the unknown NBI signal, we reserve a subset of data points in $\mathbf{x}_u$ that are randomly chosen and index this subset using $\mathcal{T}_u$. Using a binary selection matrix of size $|\mathcal{T}_u| \times P$, we can extract the portion of the received signal that corresponds to the reserved tones. The selection matrix $\mathbf{S}_{\mathcal{T}_u}$ is a partial identity matrix with only the rows that correspond to the locations of the reserved tones. Using the selection matrix on (4.9) to project $\hat{\mathbf{x}}_u$ onto the subspace spanned by the reserved points, we get

$$\begin{aligned} \underbrace{\mathbf{S}_{\mathcal{T}_u}\hat{\mathbf{x}}_u}_{\mathbf{x'}_{u,\mathcal{T}}} &= \mathbf{S}_{\mathcal{T}_u}\mathbf{x}_u + \underbrace{\mathbf{S}_{\mathcal{T}_u}\mathbf{E}_u}_{\boldsymbol{\Psi}_{u,\mathcal{T}}}\underbrace{(\boldsymbol{\mathcal{I}} + \mathbf{Z})}_{\boldsymbol{\mathcal{I}'}}, \\ &\implies \mathbf{x'}_{u,\mathcal{T}} = \boldsymbol{\Psi}_{u,\mathcal{T}}\boldsymbol{\mathcal{I}'} \end{aligned} \tag{4.10}$$

where $\mathbf{S}_{\mathcal{T}_u}\mathbf{x}_u = 0$. At this point, we have $\mathbf{x'}_{\mathcal{T}} = \boldsymbol{\Psi}_{\mathcal{T}}\boldsymbol{\mathcal{I}'}$ (we drop the subscript u for notational convenience) which represents an under-determined system of equations that can be solved using any CS recovery algorithm to find the sparse unknown $\boldsymbol{\mathcal{I}'}$. The recovery method that we use in this work is the Bayesian sparse recovery to estimate the unknown NBI signal. Generally Bayesian schemes assume the knowledge of the distribution of the active elements [13], [37]. However, in this work we use a Bayesian approach that

works with no assumption of the distribution of active elements [16]. In the following subsection we explain how this problem is addressed.

4.3.1 Prior on $\mathcal{I}'$

Although the Bayesian schemes commonly assumes a known prior on the unknown signal, [16] proposes a Bayesian scheme that is agnostic to the distribution of active taps. This scheme is known as SABMP which only acknowledges the sparsity of the unknown signal and Gaussianity of the additive noise. SABMP has further been shown to outperform many other algorithms in terms of both recovery accuracy and computational complexity [16], and is successfully utilized in several applications e.g., [38, 39]. Another advantage of SABMP is its extension for MMV, known as SABMP-MMV [40]. The SABMP-MMV is employed in the case of SIMO systems (explained in the later section).

4.4 Data-aided Recovery Using Reliable Carriers

So far, we have relied on reserved tones for recovery. To improve the recovery accuracy and spectral efficiency we seek to decrease the number of reserved tones and compensate for that using a data-aided approach. From reserved tones we found an NBI estimate and we subtract it from (4.9) resulting in

$$\hat{\mathbf{x}}_u = \mathbf{x}_u + \mathbf{E}_u \underbrace{(\boldsymbol{\mathcal{I}}' - \hat{\boldsymbol{\mathcal{I}}}')}_{\tilde{\boldsymbol{\mathcal{I}}}} = \mathbf{x}_u + \mathbf{d}_u, \tag{4.11}$$

where $\mathbf{d}_u = \mathbf{E}_u\tilde{\boldsymbol{\mathcal{I}}}'$ and it is called the residual NBI. It is understood that the residual NBI is relatively weak and a good number of data points lie in the correct decision region. Hence, we can make use of these data points to further reduce the residual NBI. And since the NBI has only few active elements, we only need a few sub-carriers to sense it. So we look for the carriers that have a high probability of falling in their correct decision region. To approach this we first start with finding the subset of reliable data carriers. [1]

Here we use the idea of remodeling $\hat{\mathbf{x}}_u$ from (4.11) i.e., $\lfloor\hat{\mathbf{x}}_u\rfloor$, where $\lfloor.\rfloor$ denotes rounding to the nearest constellation point. The sub-carriers that have residual NBI strong enough to take them out of their correct decision region i.e., $\lfloor\hat{\mathbf{x}}_u\rfloor \neq \hat{\mathbf{x}}_u$ are considered not reliable. Only the sub-carriers that satisfy $\lfloor\hat{\mathbf{x}}_u\rfloor = \hat{\mathbf{x}}_u$ are considered reliable carriers. Hence, the following reliability metric can be used

$$\mathfrak{R}(\mathbf{i}) = |\lfloor\hat{\mathbf{x}}(i)\rfloor - \hat{\mathbf{x}}(i)| \tag{4.12}$$

From the metric we know that the higher the value of $\mathfrak{R}$ the less probability of staying in the correct decision region and hence the less reliability of the sub-carrier. Therefore, we ascend the vector $\mathfrak{R}$ and choose the first $\mathcal{R}$ and find their corresponding sub-carriers that are, with high probability, reliable.

Now that we have formed the subset of reliable carriers, we seek to use them in conjunction with the reserved tones to improve the recovery accuracy.

[1] Note that the concept of using reliable carriers in multiple carrier communications is not limited to NBI mitigation [8] and has been used in applications as diverse as power amplifier linearization [41] and channel estimation [42,30].

We do that by using the selection matrix that corresponds to the new set of measurements $\mathcal{R}$, $\mathbf{S}_{\mathcal{R}}$, in (4.9). We obtain the following

$$\begin{aligned} \mathbf{S}_{\mathcal{R}}\hat{\mathbf{x}}_u &= \mathbf{S}_{\mathcal{R}}\mathbf{x}_u + \mathbf{S}_{\mathcal{R}}\mathbf{E}_u(\boldsymbol{\mathcal{I}} + \mathbf{Z}), \\ \Longrightarrow \underbrace{\mathbf{S}_{\mathcal{R}}\hat{\mathbf{x}}_u - \mathbf{S}_{\mathcal{R}}\mathbf{x}_u}_{\mathbf{x'}_{\mathcal{R}}} &= \underbrace{\mathbf{S}_{\mathcal{R}}\mathbf{E}_u}_{\boldsymbol{\Psi}_{\mathcal{R}}}\underbrace{(\boldsymbol{\mathcal{I}} + \mathbf{Z})}_{\boldsymbol{\mathcal{I}'}}, \end{aligned} \tag{4.13}$$

where the selection matrix $\mathbf{S}_{\mathcal{R}}$ is a partial identity matrix with only the rows that correspond to the locations of the reliable tones i.e., $|\mathcal{R}| \times P$. This formula has the same form as (4.10) and can be written as $\mathbf{x'}_{\mathcal{R}} = \boldsymbol{\Psi}_{\mathcal{R}}\boldsymbol{\mathcal{I}'}$. Hence, given the measurement vector $\mathbf{x'}_{\mathcal{R}}$ we can now increase the number of measurements in (4.10) by adding (4.13) to it in the following fashion

$$\underbrace{\begin{bmatrix} \mathbf{x'}_{\mathcal{T}} \\ \mathbf{x'}_{\mathcal{R}} \end{bmatrix}}_{\mathbf{x'}} = \underbrace{\begin{bmatrix} \boldsymbol{\Psi}_{\mathcal{T}} \\ \boldsymbol{\Psi}_{\mathcal{R}} \end{bmatrix}}_{\boldsymbol{\Psi}} \boldsymbol{\mathcal{I}'}, \Longrightarrow \mathbf{x'} = \boldsymbol{\Psi}\boldsymbol{\mathcal{I}'}. \tag{4.14}$$

Now (4.14) has $|\mathcal{T}| + |\mathcal{R}|$ equations as oppose to (4.10) that had only $|\mathcal{T}|$ equations. Therefore, it is expected that the solution provided from (4.14) will be an improved NBI estimate.

4.5 Multiple Antenna Base-station

In this section, we look at the case of multiple receiving antennas on the BS i.e., a SIMO setup. So each antenna will receive the same transmitted signal impaired by the NBI sources. Although, the magnitude of the NBI on the data signal may vary across the antennas, it is expected that the NBI vectors share a common support i.e., the locations of active elements in NBI vectors

across antennas do not change. This is expected as the data will arrive at different antennas through different channels. So for a V antenna system, we will have V equations of the form (4.14). Thus we have

$$\begin{aligned} \mathbf{x'}_1 &= \mathbf{\Psi}_1 \boldsymbol{\mathcal{I}'}_1 \\ \mathbf{x'}_2 &= \mathbf{\Psi}_2 \boldsymbol{\mathcal{I}'}_2 \\ &\vdots \\ \mathbf{x'}_V &= \mathbf{\Psi}_V \boldsymbol{\mathcal{I}'}_V \end{aligned} \tag{4.15}$$

where $\mathbf{x'}_v$, $\mathbf{\Psi}_v$, and $\boldsymbol{\mathcal{I}'}_v$ represent the measurement vector, sensing matrix, and the unknown NBI signal belonging to antenna v respectively. As observed from (4.14) and (4.15), we combine both the data-aided approach in the SIMO system developed to further enhance the recovery process. Here, we achieve this via the MMV version of SABMP proposed in [38]. The MMV-SABMP approach is to find the support of the unknown signal collaboratively based on all measurement vectors and later estimate the amplitudes of the active elements individually for each unknown vector.

4.6 Simulation Results

An SC-FDMA system with $N = 512$ subcarriers is simulated, with $U = 2$ active users accessing the frequency resources. The channel length is $N_c = \frac{N}{4}$ and a 16-QAM modulation is used. The NBI vector $\boldsymbol{\mathcal{I}}_L$ is generated from a complex normal distribution with SIR $= -10$ dB. We assume a maximum of four NBI sources per symbol.

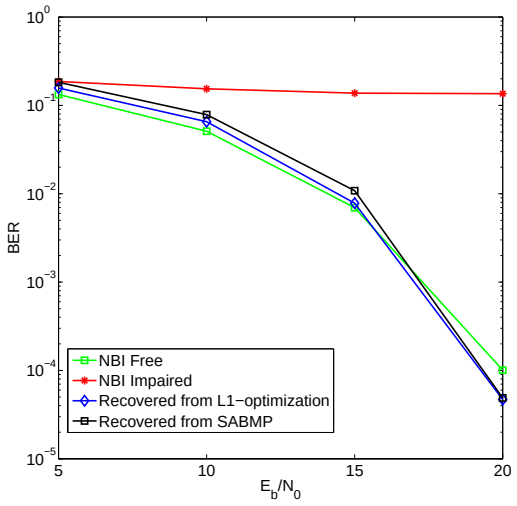

Figure 4.1: BER performance of the SABMP recovery scheme as a function of E_b/N_0 with $|\mathcal{T}| = 64$.

Figure 4.1 shows the BER results as a function of energy per bit (E_b/N_0) with 64 reserved tones per user. The results show that the SABMP scheme is effectively recovering the NBI. We also observe that for higher values of E_b/N_0 the SABMP recovery has lower BER than the NBI free case due to noise cancellation. The MMSE-FDE deals with the noise reconstruction especially for relatively weaker channels, hence showing improvement in the recovery process in comparison with the NBI free case for higher E_b/N_0. One can observe that ℓ_1- minimization has a performance that is comparable to SABMP, but this comes at the expense of very high computational complexity. Optimization schemes are much more complex than Bayesian schemes [16].

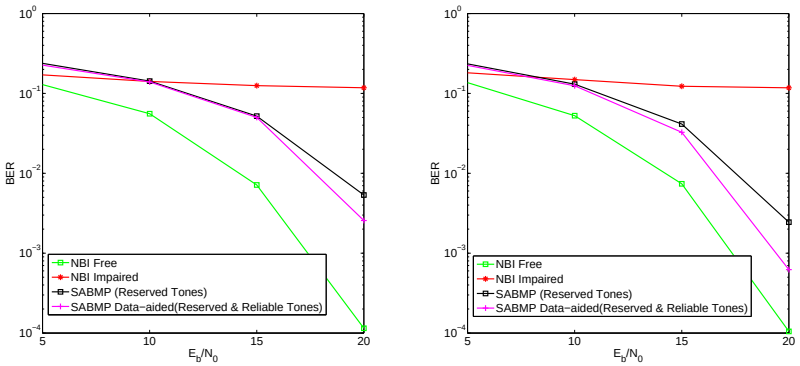

(a) $|\mathcal{T}| = 24$ and $|\mathcal{R}| = 24$ (b) $|\mathcal{T}| = 32$ and $|\mathcal{R}| = 32$

Figure 4.2: BER performance of the data-aided version of the SABMP recovery scheme as a function of E_b/N_0 with varying the values of the reserved tones $|\mathcal{T}|$ and reliable tones $|\mathcal{R}|$.

In figure 4.2, we show the case of data-aided SABMP recovery. Instead of relying on a relatively big number of reserved tones, we can decrease the number of reserved tones and compensate that by using reliable carriers along with the reserved tones to enhance the system spectral efficiency. Figure 4.2 (a) has $|\mathcal{T}| = 24$ reserved tones and $|\mathcal{R}| = 24$ reliable carriers whereas in figure 4.2 (b) we increased the number of both reserved tones and reliable carriers to $|\mathcal{T}| = 32$ and $|\mathcal{R}| = 32$. Figure 4.2 (b) shows relatively better performance of the SABMP Data-aided recovery than figure 4.2 (a). And this can be expected due to the increase in the number of reserved terms as well as the overall number of measurement data for the CS model to recover. As observed from both figure 4.2 (a) and (b), the data-aided case shows better performance than the case of relying on reserved tones only i.e., figure 4.1.

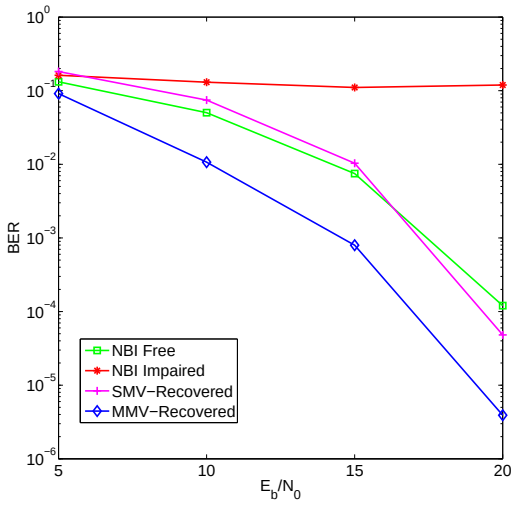

Figure 4.3: BER performance of the MMV based reconstruction of the jointly-sparse NBI signal as a function of E_b/N_0 with $|\mathcal{T}| = 64$.

In figure 4.3, we compare the performance of MMV based NBI reconstruction with SMV based reconstruction. The number of receiver antennas is 2 and received signals are combined using MRC [43]. It can be seen that the MMV reconstruction outperforms the SMV throughout the range of interest. This is expected as the antennas do collaborate to identify the active locations in the NBI signal making their decision of the active locations with high probability correct. This keeps each antenna responsible for the recovery of the values of those active locations.

In figure 4.4, we also show the data-aided case with MMV reconstruction to further enhance the spectral efficiency of the multiple receiver antennas system. It can be observed that the data-aided MMV improves the BER over the MMV recovery throughout the range of interest.

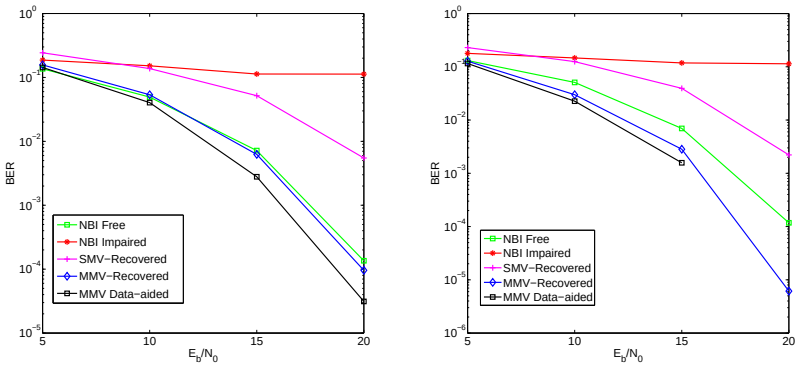

(a) $|\mathcal{T}| = 24$ and $|\mathcal{R}| = 24$ (b) $|\mathcal{T}| = 32$ and $|\mathcal{R}| = 32$

Figure 4.4: BER performance of the data-aided version of the MMV based reconstruction of the jointly-sparse NBI signal as a function of E_b/N_0 with varying the values of the reserved tones $|\mathcal{T}|$ and reliable tones $|\mathcal{R}|$.

4.7 Conclusion

A low complexity sparse reconstruction scheme has been used to estimate and mitigate the NBI effect on SC-FDMA signals. The SABMP scheme was found to be low in estimation errors compared to the ℓ_1- minimization. In addition, a data-aided approach was presented to maximize the spectral efficiency of SABMP. The scheme was also extended to the practical case of multiple receiver antennas using MMV-SABMP. This extension was found to have improvement in the NBI signal reconstruction. The data-aided approach was also implemented in this case resulting in further improvement in the NBI mitigation.

Chapter 5

Conclusions and Future Work

In this chapter, we summarize the main concepts and contributions of this thesis. In addition, we highlight some future research directions related to our work.

5.1 Conclusions

In this work, we have focused on combating specific impairments in some multi-carrier systems in order to achieve better and efficient data transmission. These impairments share the sparsity property, allowing us to use CS tools to recover these impairments and mitigate their effect. As it was mentioned in the introduction, we tackled three multi-carrier systems and their impairments; high PAPR in OFDM, self-inflected clipping distortions in OFDMA, and NBI in SC-FDMA.

In chapter 2 we used the clipping technique for PAPR reduction. In return, this technique causes inband distortions that result in compromised

performance. Therefore, we utilized the sparsity of the clipping distortion to recover it using a low complexity CS algorithm called IT. We augmented the IT algorithm with feasible phase information of the sparse signal to further enhance the reconstruction of the signal. Afterwards, we employed a data-aided approach that makes the CS model depend solely on reliable tones instead of sending pilots, in order to increase the spectral efficiency of the system. To investigate the recovery performance of the algorithm we proposed, we compared it to another recovery scheme ItML (known for its accurate recovery). Also, we adapted our algorithm to a SIMO scenario making the CS algorithm take advantage of additional measurements for better estimation. In our simulation results, we applied the algorithm in the different environments we created, for better recovery, and we showed that the IT is indeed an effective recovery scheme for clipping in OFDM and the more we take advantage of feasible and additional information the better the algorithm performs.

Chapter 3 proved self-inflected clipping distortions when in an interleaved carrier assignment in OFDMA is used. In chapter 3, we showed a mathematical proof authenticating the observation of self-inflected clipping distortions in interleaved OFDMA. In the simulation results, we deployed the CS recovery scheme FBMP for clipping recovery in the interleaved OFDMA. Our numerical results were aligned with the theoretical observations and proved that simple CS recovery is sufficient for interleaved OFDMA.

Chapter 4 addressed the NBI effect in SC-FDMA systems. In chapter 4, we utilized the sparsity of the NBI signal in the frequency domain to recover it using the low complexity sparse reconstruction scheme SABMP. As an

attempt to maximize the spectral efficiency of SABMP, we employed a data-aided approach. To investigate the recovery performance of the SABMP, we compared it to the ℓ_1- minimization. Furthermore, we adapted the scheme to the practical case of multiple receiver antennas using MMV-SABMP. In our numerical results, we applied the SABMP recovery in the different cases we simulated and found that the NBI effect on SC-FDMA was effectively mitigated.

The overall conclusion of this work is that low complexity CS tools can be used to combat the different impairments in multi-carrier systems.

5.2 Future Work

The proposed work can be extended and enriched in order to achieve higher reliability in the aforementioned multi-carrier systems. For example, one can focus on the severe out of band distortions caused by serious clipping (clipping at a low threshold). To tackle this problem we can merge clipping with some other PAPR reduction scheme. Other PAPR reduction schemes, besides clipping, limit the amplitude of the signal but not to the extent of meeting the threshold required. Hence, one can use one of those PAPR reduction schemes and then apply clipping. In return, the out of band distortions will be minimal due to the minor clipping.

Another extension, is to study the NBI effect from the point of view of several infected base stations instead of one. When and if the NBI source is effecting users from different base stations, base stations can communicate to make a better estimation of the NBI signal, since NBI is expected to share the

same support of active sources over all effected base stations. Fortunately, a distributed version of SABMP has been developed that could be adapted to the NBI in SC-FDMA problem. Even so, we can further extend this work to multiple receiver antennas on each base station increasing the estimation success.

Another impairment that effects OFDM is impulse noise. Impulse noise can be viewed as impulses occurring at random times, with short duration and high power. Hence, the impulse noise is sparse by nature in the time domain. In return, one can use IT or other low complexity sparse reconstruction tool to reconstruct and mitigate the impulse noise. Although impulse noise is similar to the PAPR reduction problem in chapter 2, there are a couple of fundamental differences/problems that need to be taken care of. First problem is that the impulse noise comes from a source outside of the system, hence there is no control on the sparsity level of the impulse noise as oppose to clipping where you can change the clipping threshold to control the sparsity level. The second problem is that the channel from the impulse noise source to the destination is unknown. These problems make the impulse noise problem more challenging and interesting.

Bibliography

[1] D. Sinanovic, G. Sisul, and B. Modlic, "Comparison of BER characteristics of OFDM and SC-FDMA in frequency selective channels," *Systems, Signals and Image Processing (IWSSIP),* 2011 18th International Conference on , vol., no., pp.1,4, 16-18 June 2011.

[2] Y.Wu and W. Y. Zou, "Orthogonal frequency division multiplexing: A multi-carrier modulation scheme," *IEEE Trans. Consumer Electronics,* vol. 41, no. 3, pp. 392–399, Aug. 1995.

[3] W. Y. Zou and Y. Wu, "COFDM: An overview," *IEEE Trans. Broadcasting,* vol. 41, no. 1, pp. 1–8, Mar. 1995.

[4] H. Myung, J. Lim, and D. Goodman, "Single carrier fdma for uplink wireless transmission," *Vehicular Technology Magazine, IEEE,* vol. 1, no. 3, pp. 30–38, Sept 2006.

[5] B. Priyanto, H. Codina, S. Rene, T. B. Sorensen, and P. Mogensen, "Initial performance evaluation of dft-spread ofdm based sc-fdma for utra lte uplink," in *Vehicular Technology Conference, 2007. VTC2007-Spring. IEEE 65th,* April 2007, pp. 3175–3179.

[6] H. Myung, J. Lim, and D. Goodman, "Peak-to-average power ratio of single carrier fdma signals with pulse shaping," in *Personal, Indoor and Mobile Radio Communications, 2006 IEEE 17th International Symposium on,* Sept 2006, pp. 1–5.

[7] K. Yamaguchi, T. Akiyama, T. Yamaguchi, T. Nagahashi, and H. Matsue, "Performance analysis of fast tracking equalization for SC-FDMA and OFDM systems under multipath fading environment," *Information Networking (ICOIN), 2015 International Conference on ,* vol., no., pp.277,282, 12-14 Jan. 2015

[8] A. Ali, M. Masood, M. S. Sohail, S. Al-Ghadhban and T. Y. Al-Naffouri, "Narrowband Interference Mitigation in SC-FDMA Using Bayesian Sparse Recovery", arXiv:1412.6137, 2014.

[9] E. B. Al-Safadi and T. Y. Al-Naffouri, "Peak reduction and clipping mitigation in OFDM by augmented compressive sensing," *IEEE Trans. Signal Process.,* vol. 60, no. 7, pp. 3834–3839, 2012.

[10] A. Al-Rabah, M. Masood, A. Ali, and T. Y. Al-Naffouri, "Receiver-based Bayesian PAPR reduction in OFDM," in *Proc. Eur. Signal Process. Conf.,* 2013.

[11] A. Gomaa and N. Al-Dhahir, "A sparsity-aware approach for NBI estimation in MIMO-OFDM," *IEEE Trans. Wireless Commun.,* vol. 10, no. 6, pp. 1854-1862, 2011.

[12] M. S. Sohail, T. Y. Al-Naffouri, and S. N. Al-Ghadhban, "Narrow Band Interference Cancellation in OFDM: A Structured Maximum Likelihood Approach," in *Proc. IEEE SPAWC,* 2012, pp. 45-49.

[13] S. Ji, Y. Xue, and L. Carin, "Bayesian compresive sensing," *IEEE Trans. Signal Process,* vol. 56, no. 6, pp. 2346-2356, 2008.

[14] K. K. Herrity, A.C. Gilbert, J. A. Tropp, "Sparse Approximation Via Iterative Thresholding" *Proc. IEEE Int. Conf. Acoust., Speech, Signal Process.,* vol.3, no., pp.III,III, 14-19, 2006.

[15] J. A. Tropp and AC. Gilbert, "Signal Recovery From Random Measurements Via Orthogonal Matching Pursuit," *IEEE Trans. Inf. Theory,* vol.53, no.12, pp.4655-4666, 2007.

[16] M. Masood and T. Y. Al-Naffouri, "Sparse reconstruction using distribution agnostic Bayesian matching pursuit," *IEEE Trans. Signal Process.,* vol. 61, no. 21, pp. 5298-5309, 2013.

[17] P. Schniter, L. C. Potter, and J. Ziniel, "Fast Bayesian matching pursuit," in Proc. Inform. Theory & Appl. Workshop, Feb. 2008.

[18] R. van Nee and R. Prasad, *OFDM for Wireless Multimedia Communications,* 2000: Artech House Publishers, Boston.

[19] P. Varahram, B. M. Ali, and W. Al-Azzo, "Low complexity ADRG-PTS scheme for PAPR reduction in OFDM systems," *Adv. Communic. Technol. (ICACT), 2011 13th Int. Conf.,* vol., no., pp.331-334, 2011.

[20] V. Tarokh and H. Jafarkhani, "On the computation and reduction of the peak-to-average power ratio in multicarrier communications," *IEEE Trans. Commun.,* vol. 48, no. 1, pp. 37–44, 2000.

[21] X. B. Wang, T. T. Tjhung, and C. S. Ng, "Reduction of peak-to-average power ratio of OFDM system using A companding technique," *IEEE Trans. Broadcast.,* vol. 45, no. 3, pp. 303-307, 1999.

[22] J. Tellado, "Peak to Average Power Ratio Reduction for Multicarrier Modulation," PhD thesis, University of Stanford, Stanford, 1999.

[23] S. S. Yoo, S. Yoon, S. Y. Kim, and I. Song, "A novel PAPR reduction scheme for OFDM systems: Selective mapping of partial tones (SMOP-T)," *IEEE Trans. Consumer Electronics,* vol. 52, no. 1, pp. 40–43, 2006.

[24] L. Xiaodong and L. J. Cimini, "Effects of clipping and filtering on the performance of OFDM," *Veh. Technol. Conf.,* vol.3, no., pp.1634,1638 vol.3, 1997.

[25] T. Jiang and Y. Wu, "An overview: peak-to-average power ratio reduction techniques for OFDM signals," *IEEE Trans. Broadcast.,* vol. 54, no. 2, pp. 257–268, 2008.

[26] J. Tellado et al., "Maximum-likelihood detection of nonlinearly distorted multicarrier symbols by iterative decoding," *IEEE Trans. Commun.,* vol. 51, no. 2, pp. 218-228, 2003.

[27] T. Blumensath and M. E. Davies, "Normalized Iterative Hard Thresholding: Guaranteed Stability and Performance," *IEEE J. Sel. Topics Signal Process.,* vol.4, no.2, pp.298 -309, 2010.

[28] D. Qing and Z. Hongsheng, "An Improved Algorithm to Reduce PAPR Based Clipping-and-Filtering," in *Proc. WiCOM 4th Int. Conf.,* vol., no., pp.1,4, 12-14, 2008.

[29] R. Gross and D. Veeneman, "SNR and spectral properties for a clipped DMT ADSL signal," in *Proc. SUPERCOMM/ICC Conf. IEEE Int. Conf.,* vol., no., pp.843,847 vol.2, 1994.

[30] A. Ali, A. Al-Zahrani, T. Y. Al-Naffouri and A. Naguib,, "Receiver Based PAPR Reduction in OFDMA," in *Proceedings of International Conference on Acoustics, Speech and Signal Processing (ICASSP),* 2014.

[31] E. B. Al-Safadi, T. Y. Al-Naffouri, M. Masood, and A. Ali, "Nonlinear Distortion Reduction in OFDM from Reliable Perturbations in Data Carriers".

[32] T. Blumensath and M. E. Davies, "Iterative hard thresholding for compressed sensing," *Appl. and Comput. Harmon. Anal.,* vol. 27, no. 3, pp. 265-274, 2009.

[33] H. Zhu, Z. Ji, K.J.R. Liu, "Fair Multiuser Channel Allocation for OFDMA Networks Using Nash Bargaining Solutions and Coalitions," *Communications, IEEE Transactions* on , vol.53, no.8, pp.1366,1376, Aug. 2005.

[34] G. Huang, A. Nix, and S. Armour, "Decision feedback equalization in SC-FDMA ," in *Proc. IEEE PIMRC,* 2008, pp. 1-5.

[35] H. Wang, X. You, B. Jiang, and X. Gao, "Performance analysis of frequency domain equalization in SC-FDMA systems," in *Proc. ICC'08.* IEEE, 2008, pp. 4342-4347.

[36] G. Berardinelli, B. E. Priyanto, T. B. Sorensen, and P. Mogensen, "Improving SC-FDMA performance by turbo equalization in UTRA LTE uplink," in *Proc. IEEE Veh. Technol. Conf.,* 2008, pp. 2557-2561.

[37] S. D. Babacan, R. Molina, and A. K. Katsaggelos, "Bayesian compressive sensing using Laplace priors," in *IEEE Trans. Image Process,* vol. 19, no. 1, pp. 53-63, 2010.

[38] A. Ali, A. Al-Rabah, M. Masood and T. Y. Al-Naffouri, "Receiver-based Recovery of Clipped OFDM Signals for PAPR Reduction: A Bayesian Approach", *IEEE Access,* vol. 2, pp. 1213-1224, 2014.

[39] A. Ali, O. Hammi and T. Y. Al-Naffouri, "Compressed Sensing based Joint-Compensation of Power Amplifier's Distortions in OFDMA Cognitive Radio Systems", *IEEE Journal on Emerging and Selected Topics in Circuits and Systems (JETCAS),* vol. 3, no. 4, pp. 508-520, 2013.

[40] T. Y. Al-Naffouri and M. Masood, "Distribution agnostic structured sparsity recovery algorithms," in *Proc. IEEE WoSSPA,* 2013, pp. 283-290.

[41] D. S. Owodunni, A. Ali, A. Quadeer, E. B. Al-Safadi, O. Hammi and T. Y. Al-Naffouri, "Compressed Sensing Techniques for Receiver based Post-Compensation of Transmitter's Nonlinear Distortions in OFDM Systems", *Signal Processing,* vol. 97, pp. 282-293, 2014.

[42] M. Masood, L. H. Afify, and T. Y. Al-Naffouri, "Efficient coordinated recovery of sparse channels in massive MIMO," *IEEE Trans. on Sig. Process.,* 2014.

[43] J. Boutros and E. Viterbo, "Signal space diversity: a power-and bandwidth-efficient diversity technique for the Rayleigh fading channel," *IEEE Trans. Inf. Theory,* vol. 44, no. 4, pp. 1453–1467, Jul. 1998.